9890 *Inorg. Chem.* **2009**, *48*, 9890–9903
DOI: 10.1021/ic9014288

Inorganic Chemistry
Article

Tetrakis(thiadiazole)porphyrazines. 6. Spectroelectrochemical and Density Functional Theory Studies of the Anions $[TTDPzM]^{n-}$ (n = 1−4; M = Zn^{II}, $Mg^{II}(H_2O)$, Cu^{II}, $2H^{I}$)

Maria Pia Donzello,[†] Claudio Ercolani,*[,†] Xiaohui Cai,[‡] Karl M. Kadish,*[,‡] Giampaolo Ricciardi,*[,§] and Angela Rosa*[,§]

[†]*Dipartimento di Chimica, Università degli Studi di Roma "La Sapienza", P.le A. Moro 5, Roma, I-00185, Italy,* [‡]*Department of Chemistry, University of Houston, Houston, Texas, 77204-5003, USA, and* [§]*Dipartimento di Chimica, Università della Basilicata, Via N. Sauro 85, I-85100, Potenza, Italy*

Received July 21, 2009

Following previous cyclic voltammetric studies of tetrakis(thiadiazole)porphyrazines [TTDPzM] where M = Zn^{II}, $Mg^{II}(H_2O)$, Cu^{II}, or $2H^{I}$ in nonaqueous media, a thin-layer spectroelectrochemical investigation was carried out in pyridine to characterize each stepwise one-electron reduction of the electrogenerated $[TTDPzM]^{n-}$ complexes where n = 1−4. A similar UV−visible spectrum was observed for each form of the anion, independent of the central metal ion and detailed theoretical calculations by density functional theory (DFT) and time-dependent DFT (TDDFT) methods were applied to interpret the spectral features of $[TTDPzZn]^{n-}$ (n = 1−4) which was selected as representative for describing the ground and excited-state electronic structures of the entire $[TTDPzM]^{n-}$ series. The use of two exchange-correlation functionals, the pure, asymptotically correct statistical average of orbital potentials (SAOP) and the hybrid B3LYP functionals, proved to be essential for attaining a correct assignment of the key spectral features. The nature and intensity of the main spectral features are highlighted and interpreted on the basis of the ground-state electronic structure of the complexes.

Introduction

The synthesis, structural and electronic features, and general physicochemical properties of symmetrical highly electron-deficient free-base and metalated tetrakis(thiadiazole)porphyrazines,[1] represented as [TTDPzM] (Chart 1-a; M = $2H^{I}$), their tetrakis(selenodiazole)porphyrazine analogues,[2] [TSeDPzM] (Chart 1-b; M = $2H^{I}$), and several related low-symmetry species[3] have been concisely reviewed.[4] Electrochemical and spectroelectrochemical studies were first reported for the "thiadiazoleporphyrazines" carrying tervalent metal ions. These compounds[1c] are represented as [TTDPzMX] where M = Al^{III}, Ga^{III} or In^{III} and X = Cl^{-}, Br^{-}, or CH_3COO^{-}. More recently,[5] the redox properties of [TTDPzM] where M = $2H^{I}$, $Mg^{II}(H_2O)$, Cu^{II}, or Zn^{II} were examined by cyclic voltammetry in pyridine, dimethylsulfoxide (DMSO), and *N*,*N*-dimethylformamide (DMF) and shown to undergo stepwise well-separated reversible ligand-centered one-electron reductions to give the corresponding −1, −2, −3, and −4 charged anions. The $E_{1/2}$ values for each process are remarkably less negative than values reported earlier for phthaloctanine (Pc) analogues with the same central metal ions.[6] Moreover, UV−visible spectra of the thiadiazoleporphyrazine complexes exhibit hypsochromically shifted Q and B bands and a more complex B band region as compared to the parallel series of phthalocyanines.[4b]

*To whom correspondence should be addressed. E-mail: claudio.ercolani@uniroma1.it.

(1) (a) Stuzhin, P. A.; Bauer, E. M.; Ercolani, C. *Inorg. Chem.* **1998**, *37*, 1533. (b) Bauer, E. M.; Cardarilli, D.; Ercolani, C.; Stuzhin, P. A.; Russo, U. *Inorg. Chem.* **1999**, *38*, 6114. (c) Donzello, M. P.; Agostinetto, R.; Ivanova, S. S.; Fujimori, M.; Suzuki, Y.; Yoshikawa, H.; Shen, J.; Awaga, K.; Ercolani, C.; Kadish, K. M.; Stuzhin, P. A. *Inorg. Chem.* **2005**, *44*, 8539. (d) Stuzhin, P. A.; Pozdysheva, E. A.; Mal'chugina, O. V.; Popkova, I. A.; Ercolani, C. *Chem. Heterocycl. Compd.* **2005**, 278 (Khim. Geterotsikl. Soed. 2005, 246). (e) Fujimori, M.; Suzuki, Y.; Yoshikawa, H.; Awaga, K. *Angew. Chem.* **2003**, *115*, 6043. (f) Suzuki, Y.; Fujimori, M.; Yoshikawa, H.; Awaga, K. *Chem.—Eur. J.* **2004**, *10*, 5158.

(2) (a) Bauer, E. M.; Ercolani, C.; Galli, P.; Popkova, I. A.; Stuzhin, P. A. *J. Porphyrins Phthalocyanines* **1999**, *3*, 371. (b) Angeloni, S.; Bauer, E. M.; Ercolani, C.; Popkova, I. A.; Stuzhin, P. A. *J. Porphyrins Phthalocyanines* **2001**, *5*, 881.

(3) (a) Kudrik, E. V.; Bauer, E. M.; Ercolani, C.; Stuzhin, P. A.; Chiesi-Villa, A.; Rizzoli, C. *Mendeleev Commun.* **2001**, 45. (b) Donzello, M. P.; Ercolani, C.; Gaberkorn, A.; Kudrik, E. V.; Meneghetti, M.; Marcolongo, G.; Rizzoli, C.; Stuzhin, P. A. *Chem.—Eur. J.* **2003**, *9*, 4009.

(4) (a) Stuzhin P. A., Ercolani C. *The Porphyrin Handbook*; Kadish K. M., Smith K. M., Guilard R., Eds.; Academic Press: New York, 2003, Vol. *15*, Chapter 101, pp 263−364; (b) Donzello, M. P.; Ercolani, C.; Stuzhin, P. A. *Coord. Chem. Rev.* **2006**, *250*, 1530–1561.

(5) Donzello, M. P.; Ercolani, C.; Kadish, K. M.; Ricciardi, G.; Rosa, A.; Stuzhin, P. A. *Inorg. Chem.* **2007**, *46*, 4145.

(6) Clack, D. W.; Hush, N. S.; Woolsey, I. S. *Inorg. Chim. Acta* **1976**, *19*, 129.

 Published on Web 09/17/2009

Chart 1

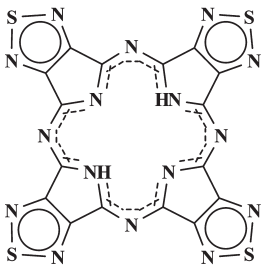

1-a

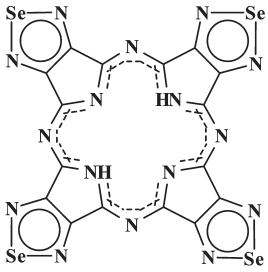

1-b

The ground- and excited-state electronic properties of compounds in the [TTDPzM] series of complexes were also studied in detail by density functional theory (DFT) and time-dependent DFT (TDDFT) methods, taking into account bulk and specific (axial ligation) solvent effects.[5] This analysis revealed that replacement of the benzo rings of the Pc macrocycle by electron-withdrawing thiadiazole rings induces a large stabilization of both the highest occupied molecular orbitals (HOMOs) and the lowest unoccupied molecular orbitals (LUMOs) in the [TTDPzM] complexes relative to the Pc analogues. An excellent correlation was found between the first one-electron reduction potentials and the LUMO energies. TDDFT calculations of the lowest excited states of the [TTDPzM] series of compounds also provided an accurate description of the UV−visible spectra and valuable information on the nature of the complexes in solution. For example, the calculated optical spectra of the free-base macrocyle are consistent with the experimental data in pyridine suggesting that in this solvent the species is mostly present in its deprotonated form as earlier reported and later discussed in more detail.[1a]

To complement our experimental and theoretical studies of neutral [TTDPzM],[5] we have now extended our efforts to include a characterization of UV−visible spectra for each anion generated after stepwise controlled potential reduction in a thin layer cell. The spectral features of electrogenerated $[TTDPzM]^{n-}$ (n = 1−4) where M = $Mg^{II}(H_2O)$, Zn^{II}, Cu^{II}, or $2H^{I}$ are reported for the first time in the present paper and interpreted on the basis of DFT/TDDFT calculations. Because the spectral changes at the various steps of reduction are similar for each compound in a given oxidation state (vide infra), as expected for ligand-centered redox processes, DFT/TDDFT studies were restricted to the anionic complexes of $[TTDPzZn]^{n-}$ (n = 1−4) which are taken as representative of the spectroelectrochemically investigated series of anions. Similarities and differences between the spectroscopic behavior of these anions in pyridine and that of their phthalocyanine analogues, for which numerous experimental and theoretical studies are available,[7] are also discussed.

Experimental Section

Syntheses of the [TTDPzM] (M = $2H^{I}$, $Mg^{II}(H_2O)$, Cu^{II}, Zn^{II}) were carried out as previously reported.[1a,b] As specified elsewhere, all of the compounds normally contain some additional clathrated water (one or two moles per mole of macrocycle) after exposure to air. The amount of water present is not rigorously defined and depends upon the specific sample and the ambient conditions.[1a,b] These water molecules were not expected (nor shown) to influence the electrochemistry of these materials in nonaqueous media,[5] and the presence of water is therefore neglected in the given formulation of each compound. The presence of a water molecule coordinated to Mg^{II} in the complex [TTDPzMg(H_2O)] was previously discussed.[5]

Spectroelectrochemical Measurements. Thin-layer spectroelectrochemical measurements were carried out in pyridine solution with an optically transparent platinum thin-layer working electrode using a Hewlett-Packard model 8453 diode array spectrophotometer coupled with an EG&G model 173 universal programmer and using 0.2 M TBAP as supporting electrolyte.

Computational Details. The ground state molecular structures of the $[TTDPzZn]^{n-}$ (n = 1−3) complexes were optimized at the BP86 level[8,9] of DFT using the Amsterdam Density Functional (ADF) program package.[10−13] For the open-shell complexes the spin-unrestricted DFT formalism was employed. Spin contamination, monitored by the $\langle S^2 \rangle$ expectation value, was found to be negligible in all cases. The calculated structures were verified to represent local minima by calculation of harmonic frequencies. Since the compounds studied in this work are anions, the geometry optimizations were also carried out in solution using the conductor-like screening model (COSMO)[14,15] as implemented in ADF[16] and using pyridine as solvent. The effects of the solvent on the predicted geometries proved to be negligible (see the Supporting Information, Table S1). Therefore, the ground- and excited-state properties were computed at the gas-phase optimized geometries. For all optimizations and frequency calculations, the extensive all electron ADF TZ2P basis set, which is an uncontracted triple-ζ STO basis set with two polarization functions, was applied. The ground state molecular structures of the $[TTDPzZn]^{n-}$ (n = 1, 3) complexes were also optimized, in the gas-phase, at the B3LYP[17−19] level of DFT using Turbomole V6.0[20,21] and the balanced basis set of triple-ζ-valence quality, def2-TZVP.[22]

Vertical absorption energies and oscillator strengths of the lowest dipole and spin allowed excited states of the $[TTDPzZn]^{n-}$ (n = 1−3) complexes were computed at the TDDFT level using the pure asymptotically correct SAOP, the statistical average of orbital potentials functional,[23,24] and the hybrid

(7) (a) Minor, P. C.; Gouterman, M.; Lever, A. B. P. *Inorg. Chem.* **1985**, *24*, 1894. (b) Nyokong, T. N.; Gasyna, Z.; Stillman, M. J. *Inorg. Chem.* **1987**, *26*, 1087. (c) Nyokong, T. N.; Gasyna, Z.; Stillman, M. J. *Inorg. Chem.* **1987**, *26*, 548. (d) Ough, E. A.; Gasyna, Z.; Stillman, M. J. *Inorg. Chem.* **1991**, *30*, 2301. (e) Mack, J.; Stillman, M. J. *J. Am. Chem. Soc.* **1994**, *116*, 1292. (f) Mack, J.; Stillman, M. J. *Inorg. Chem.* **1997**, *36*, 413. (g) Mack, J.; Stillman, M. J. *Coord. Chem. Rev.* **2001**, *219−221*, 993. (h) Mack, J.; Stillman, M. J. *The Porphyrins Handbook*; Kadish, K. M., Smith, K. M., Guilard, R., Eds.; Academic Press: New York, 2003; Vol. *16*, Chapter 103, pp 43−116. (i) Mack, J.; Kobayashi, N.; Stillman, M. J. *J. Porphyrins Phthalocyanines* **2006**, *10*, 1219. (j) Rosa, A.; Ricciardi, G. *Can. J. Chem.* **2009**, *87*, 994.

(8) Becke, A. *Phys. Rev. A* **1988**, *38*, 3098.
(9) Perdew, J. P. *Phys. Rev. B* **1986**, *33*, 8822.
(10) *ADF2008.01*; SCM, Theoretical Chemistry, Vrije Universiteit: Amsterdam, The Netherlands; available from http://www.scm.com.
(11) Baerends, E. J.; Ellis, D. E.; Ros, P. *Chem. Phys.* **1973**, *2*, 41.
(12) Fonseca Guerra, C.; Snijders, J. G.; te Velde, G.; Baerends, E. J. *Theor. Chem. Acc.* **1998**, *99*, 391.
(13) te Velde, G.; Bickelhaupt, F. M.; Baerends, E. J.; Fonseca Guerra, C.; van Gisbergen, S. J. A.; Snijders, J. G.; Ziegler, T. *J. Comput. Chem.* **2001**, *22*, 931.
(14) Klamt, A.; Schürmann, G. *J. Chem. Soc., Perkin Trans.* **1993**, *2*, 799.
(15) Klamt, A.; Jonas, V. *J. Chem. Phys.* **1996**, *105*, 9972.
(16) Pye, C. C.; Ziegler, T. *Theor. Chem. Acc.* **1999**, *101*, 396.
(17) Becke, A. D. *J. Chem. Phys.* **1993**, *98*, 5648.
(18) Lee, C.; Yang, W.; Parr, R. G. *Phys. Rev. B* **1988**, *37*, 785.
(19) Stephens, P. J.; Devlin, F. J.; Chabalowski, C. F.; Frisch, M. J. *J. Phys. Chem.* **1994**, *98*, 11623.
(20) Ahlrichs, R.; Bär, M.; Häser, M.; Horn, H.; Kölmel, C. *Chem. Phys. Lett.* **1989**, *162*, 165.
(21) Bauernschmitt, R.; Ahlrichs, R. *Chem. Phys. Lett.* **1996**, *256*, 454.
(22) Weigend, F.; Ahlrichs, R. *Phys. Chem. Chem. Phys.* **2005**, *7*, 3297.
(23) Gritsenko, O. V.; Schipper, P. R. T.; Baerends, E. J. *Chem. Phys. Lett.* **1999**, *302*, 199.
(24) Schipper, P. R. T.; Gritsenko, O. V.; van Gisbergen, S. J. A.; Baerends, E. J. *J. Chem. Phys.* **2000**, *112*, 1344.

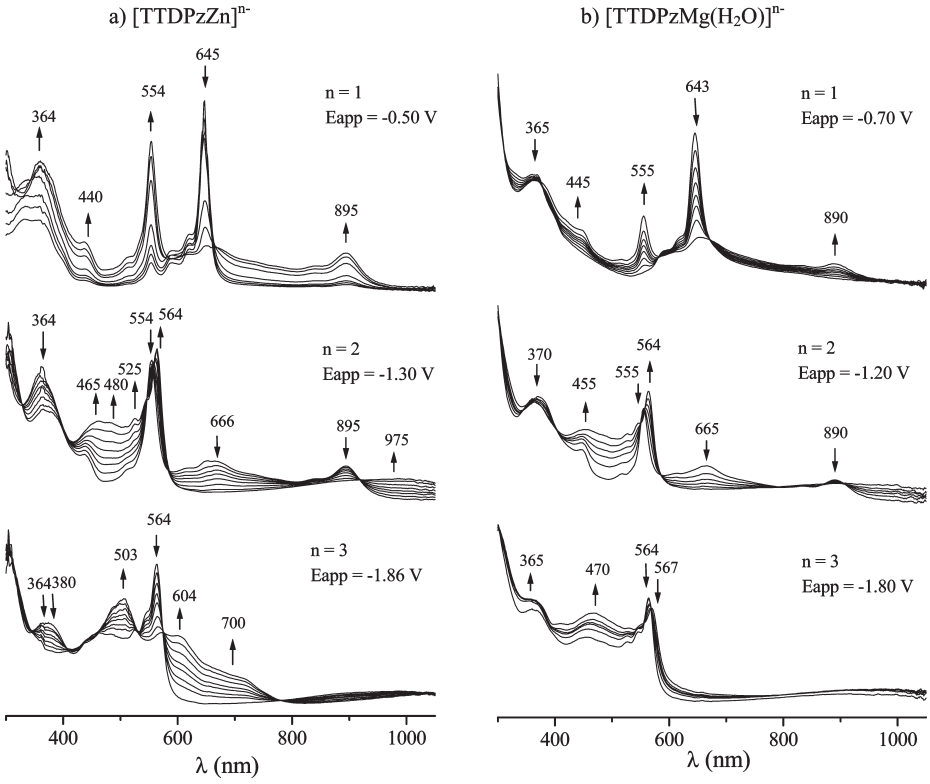

Figure 1. UV−visible spectral changes for generation of (a) $[TTDPzZn]^{n-}$ and (b) $[TTDPzMg(H_2O)]^{n-}$ where $n = 1$ to 3 in pyridine containing 0.2 M TBAP during controlled potential reductions at indicated potentials. The $E_{1/2}$ for each process is given in ref 5.

B3LYP functional. TDDFT/SAOP calculations were performed with ADF using the same all electron TZ2P basis set used in the DFT calculations. TDDFT/B3LYP calculations were carried out with Turbomole V6.0 using the def2-TZVP basis set.

Solvent effects on the excitation energies were modeled by the conductor-like continuum solvent model (COSMO).[15,16]

Results and Discussion

Spectroelectrochemical Measurements. As reported earlier,[1a,b,5] the UV−visible spectra of unreduced [TTDPzM] in nonaqueous media show an expected pattern for phthalocyanine and porphyrazine macrocycles, that is, a $\pi-\pi^*$ transition in the Soret bands region (380−300 nm) and a more intense Q-band at 630−690 nm. The sharpness of the Q band for the four neutral compounds and the lack of any broad bands which can be attributed to aggregation indicates that these macrocycles are preponderantly present in their monomeric form at about 10^{-5} M concentration. This is not the case at the higher concentration of $10^{-4}-10^{-3}$ M which is needed for thin-layer spectroelectrochemistry and here it was necessary to "solubilize" the material by first scanning to negative potentials to generate the more soluble anions and then reverse the potential to 0.0 V to observe the neutral spectrum of the monomeric complex after which more negative potentials were applied to elucidate the UV−visible properties of each reduced form in the absence of aggregation. In this way quantitative spectroelectrochemical experiments could be carried out on these compounds which would not be possible when starting from the neutral form. This method allowed us to measure not only wavelength maxima but also molar absorptivities for the first three forms of the generated anions. It should be noted that the fourth reduction occurred quite close to the potential limit of the solvent, thus making it difficult to obtain meaningful spectral changes in these cases.

Examples of the UV−visible spectra obtained during reduction of [TTDPzM] in pyridine are shown in Figures 1 and 2, and a summary of the data is given in Table 1. The potentials of each redox process are reported in the literature[5] and also summarized in Supporting Information, Table S1. As seen in the figures, several isosbestic points are obtained for each transition, indicating the lack of spectral intermediates. The UV−visible spectra of each $[TTDPzM]^{n-}$ anion generated at the various steps of reduction are similar to each other and independent of the central metal (see Table 1), which is not unusual since all reductions are ligand-centered. For example, the most intense band of the monoanion is located at 554, 555, and 550 nm for the Zn^{II}, Mg^{II}, and Cu^{II} complexes, respectively, while in the case of the dianion, the most intense band for the same three compounds is located at 564, 564, and 563 nm as seen in Table 1.

The lack of significant dependence of the central metal ion on the UV−visible spectra of the anions closely resembles what was reported for a related series of porphyrazine derivatives carrying peripherally annulated seven membered diazepine rings[25] or the dipyridinopyrazine fragments.[26] The observed common spectral

(25) Donzello, M. P.; Dini, D.; D'Arcangelo, G.; Zhan, R.; Ou, Z.; Ercolani, C.; Stuzhin, P. A.; Kadish, K. M. *J. Am. Chem. Soc.* **2003**, *125*, 14190.

(26) (a) Donzello, M. P.; Ou, Z.; Monacelli, F.; Ricciardi, G.; Rizzoli, C.; Ercolani, C.; Kadish, K. M. *Inorg. Chem.* **2004**, *43*, 8626. (b) Donzello, M. P.; Ou, Z.; Dini, D.; Meneghetti, M.; Ercolani, C.; Kadish, K. M. *Inorg. Chem.* **2004**, *43*, 8637. (c) Bergami, C.; Donzello, M. P.; Monacelli, F.; Ercolani, C.; Kadish, K. M. *Inorg. Chem.* **2005**, *44*, 9862. (d) Donzello, M. P.; Viola, E.; Cai, X.; Mannina, L.; Rizzoli, C.; Ricciardi, G.; Ercolani, C.; Kadish, K. M.; Rosa, A. *Inorg. Chem.* **2008**, *47*, 3903.

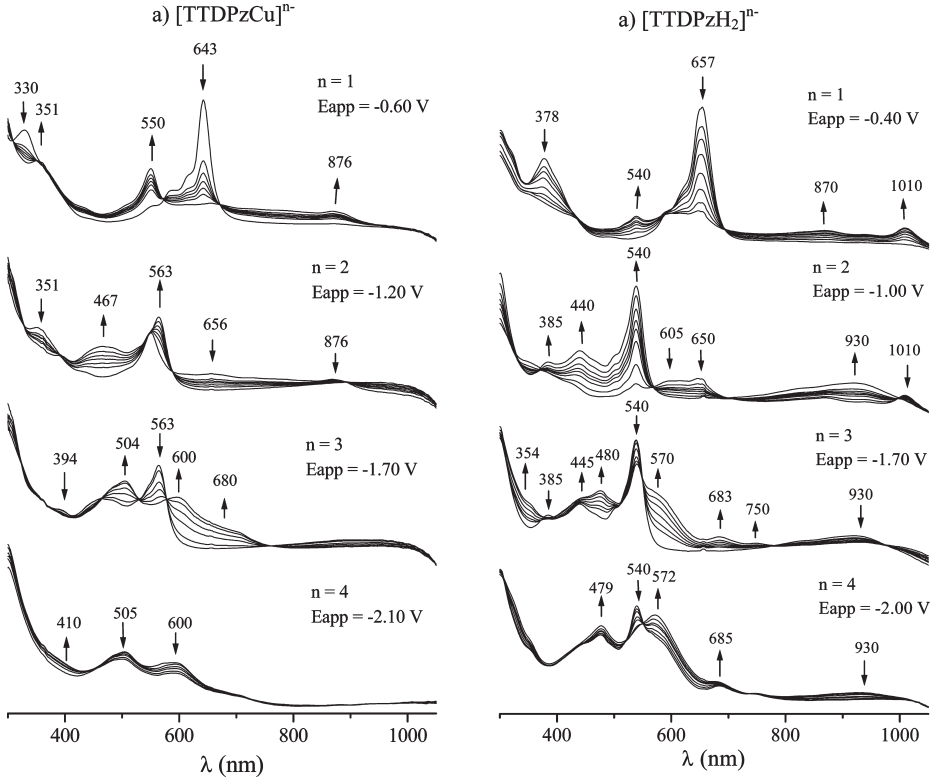

Figure 2. UV−visible spectral changes for generation of (a) $[TTDPzCu]^{n-}$ and (b) $[TTDPzH_2]^{n-}$ where n = 1 to 4 in pyridine containing 0.2 M TBAP during controlled potential reductions at indicated potentials. The $E_{1/2}$ for each process is given in ref 5.

Table 1. UV-visible Spectral Data [λ (nm), log ε] for Neutral [TTDPzM] and Electroreduced $[TTDPzM]^{n-}$ (n = 1−4) in Pyridine

	λ (nm)						
compound	Soret region			Q-band region			
[TTDPzZn]	335 (4.94); 359 (4.86)	440(sh)	554; 592 (4.48)	625 (sh)	645 (5.31)		
$[TTDPzZn]^{1-}$	364 (4.82)	440 (4.34); 515 (sh)	554 (4.87)		666 (4.36)	837; 895 (4.26)	
$[TTDPzZn]^{2-}$	364 (4.75); 380 (4.72)	465 (4.61); 480 (sh)	548 (sh); 564 (4.92)				~975
$[TTDPzZn]^{3-}$	360 (sh)	505 (4.83)	572 (4.67)	604 (4.68)	700 (sh) (4.38)		~1100
$[TTDPzMg(H_2O)]$	365 (4.87)		590 (4.36)	620 (sh) (4.53)	643 (5.15)		
$[TTDPzMg(H_2O)]^{1-}$	370 (4.82)	445 (sh) (4.46)	555 (4.79)		665 (4.36)	890 (4.27)	
$[TTDPzMg(H_2O)]^{2-}$	363 (4.73)	455 (4.61)[a]	564 (4.82)				
$[TTDPzMg(H_2O)]^{3-}$	365 (4.74)	470 (4.74)[a]	567 (4.75)				~1100
[TTDPzCu]	330 (4.75)		560 (sh); 590 (4.24)	618 (sh) (4.45)	643 (5.01)		
$[TTDPzCu]^{1-}$	351 (4.60)		550 (4.51)			876 (3.88)	
$[TTDPzCu]^{2-}$	394	467 (4.43)	563 (4.60)				
$[TTDPzCu]^{3-}$		504 (4.57)		600 (4.43)	680 (sh)		
$[TTDPzCu]^{4-}$		505 (4.58)	585 (4.20)		695 (sh)		~1100
$[TTDPzH_2]$	378 (4.82)		595 (sh) (4.34)	620 (sh) (4.59)	657 (5.02)		
$[TTDPzH_2]^{1-}$			540 (4.46)	605 (4.42)[a]	650 (4.42)	870 (3.98)[a]	1010
$[TTDPzH_2]^{2-}$	385 (4.56)	440 (4.66)	540 (5.00)				930[a]
$[TTDPzH_2]^{3-}$	354 (sh) (4.78)	445 (sh); 480 (4.86)	540 (4.81); 570 (sh) (4.89)		683 (4.38)		
$[TTDPzH_2]^{4-}$		479 (4.75)	550 (sh); 572 (4.54)		685 (sh)		

[a] broad.

changes for the all four species at each individual step of reduction are summarized below:

First Reduction. (a) Complete disappearance of the Q band (643−657 nm) with an appearance of absorptions at 540−555 and 870−895 nm; (b) decrease of intensity of band in the Soret region with a slight shift to lower energy.

Second Reduction. (a) Increase in intensity of the 540−555 nm absorption with a slight shift to 563−564 nm ($Mg^{II}(H_2O)$, Cu^{II}, Zn^{II}) or unmoved ($2H^{I}$: 540 nm); (b) disappearance of the 870−895 nm absorptions and appearance of broad absorptions in the range 430−480 nm.

Third Reduction. (a) Disappearance 563−564 nm ($Mg^{II}(H_2O)$, Cu^{II}, Zn^{II}) or 540 nm ($2H^{I}$) absorptions with concomitant increase in intensity of the 470−504 and 570−604 nm.

Fourth Reduction. Only minor changes.

Quantum Chemical Calculations of $[TTDPzZn]^{n-}$ (n = 1−4). To afford an accurate description of the electronic

absorption spectra of the $[TTDPzZn]^{n-}$ ($n = 1-4$) anions, taken as representative of the entire series, we examine in this section the excited states of these species using TDDFT methods. Before dealing with the excited states of the anions we elucidate, through DFT calculations, their ground-state molecular and electronic structure.

Molecular Structure. Each compound in the [TTDPzM] series was electrochemically reduced to give the negative ions $[TTDPzM]^{n-}$ ($n = 1-4$). As in the case of metal phthalocyanine analogues with electroinactive metals, [PcM],[27,7] electron addition is confined to the π orbitals of the macrocycle. Up to four electrons can be reversibly added to the LUMOs, the 2-fold degenerate e_g* MOs in the D_{4h} molecular structure of [TTDPzM].[5]

Addition of one electron to the e_g* LUMOs of neutral [TTDPzZn] results in the 2-fold degenerate ^2E_g state. Therefore, a Jahn−Teller (JT) distortion will take place to remove this electronic degeneracy. According to general theory,[28,29] the JT-active coordinates are of either B_{1g} or B_{2g} symmetry resulting in D_{2h} configurations of a *diamond* (rhombus) or *rectangle*, respectively. Geometry optimization of $[TTDPzZn]^{\bullet-}$ in the gas-phase leads to a D_{2h} *diamond* structure with a $^2B_{3g}$ electronic ground state. The D_{2h} *rectangular* structure, which is only 0.1 kJ/mol less stable, has an imaginary frequency (107 cm^{-1}) of B_{1g} symmetry. At variance with $[TTDPzZn]^{\bullet-}$, $[PcZn]^{\bullet-}$,[7j] and $[PcMg]^{\bullet-}$[30] distort to a D_{2h} *rectangular* structure. The energy gap between the two JT-distorted structures of $[TTDPzZn]^{\bullet-}$ also remains quite small (0.7 kJ/mol) when the calculations are performed at the B3LYP/TZVP level of theory. A value of 0.5 kJ/mol has been reported for the JT-distorted structures of $[PcZn]^{\bullet-}$[8j] and values in the range of 0−3 kJ/mol have been reported by Nguyen and Pachter[31] for the JT-distorted triplet state structures of a series of zinc tetrapyrroles, including PcZn.

The dianionic species $[TTDPzZn]^{2-}$ has a $(e_g^*)^2$ ground state configuration, which generates multideterminantal configuration state functions, that is, a triplet state, the $^3A_{2g}$, and three singlet states, the $^1A_{1g}$, $^1B_{1g}$, and $^1B_{1g}$. Which of these states is the ground state of the dianion cannot be established using DFT. Within a monodeterminantal approach such as DFT it is not always possible, particularly in an high point group symmetry, to resolve all multiplets of a given configuration from the energies of single determinants only. When possible, one would only get the *unrelaxed* total energy of the state. The ground state of $[TTDPzZn]^{2-}$should be, in principle, the triplet state. However, for the dianion of the unsubstituted and octacyano-substituted phthalocyanine analogues, $[PcZn]^{2-}$ and $[Pc(CN)_8Zn]^{2-}$, electron paramagnetic resonance (EPR) experiments point to a singlet ground state.[32] This was explained by Minor et al.[7a] by invoking a *pseudo* JT effect that would stabilize one of the singlet states, namely, the $^1B_{1g}$, with respect to the $^3A_{2g}$.[7a] Unfortunately, EPR data are not available for $[TTDPzZn]^{2-}$. However, it is reasonable to assume that this species has a singlet ground state, just as $[PcZn]^{2-}$[32a] and $[Pc(CN)_8Zn]^{2-}$.[32b,c] Actually, according to redox data, $[Pc(CN)_8Zn]$ shares with [TTDPzZn] a remarkable electron-deficient character. As $[TTDPzZn]^{2-}$ is generated by one-electron reduction of the monoanion, the simplest way to obtain a singlet ground state is to pair the two electrons in the lower-energy JT-split LUMO of $[TTDPzZn]^{\bullet-}$. Thus, starting from the ground-state D_{2h} *diamond* structure of the monoanion, we carried out a geometry optimization of $[TTDPzZn]^{2-}$ under D_{2h} symmetry and with a $(b_{3g})^2$ closed-shell configuration. The resulting structure had an imaginary frequency (294 cm^{-1}) of B_{1g} symmetry. The geometry was therefore distorted along the eigenvector representing the imaginary frequency and reoptimized, and the frequencies were recalculated. Theoretical results showed that the minimum corresponds to a D_{2h} *rectangular* structure.

The third reduction step generates the π radical trianionic species, $[TTDPzZn]^{\bullet3-}$, with $(e_g^*)^3$ configuration. This configuration gives rise to a ^2E_g state, which should undergo a JT distortion as in the monoanion. Geometry optimization of the trianionic species in the gas-phase led to a D_{2h} *diamond* structure with a $^2B_{2g}$ electronic ground state. The D_{2h} *rectangular* structure, which is 0.8 kJ/mol higher in energy (1.2 kJ/mol at B3LYP/TZVP level of theory), showed an imaginary frequency (472 cm^{-1}) of B_{1g} symmetry. The fourth reduction fills the e_g* and $[TTDPzZn]^{4-}$ has a D_{4h} symmetry molecular structure and a $^1A_{1g}$ electronic ground state.

Table 2 lists the most relevant bond parameters calculated for the $[TTDPzZn]^{n-}$ ($n = 1-4$) series of anions and, for sake of comparison, those previously reported for the neutral complex, [TTDPzZn].[5] The labeling of the nonequivalent atomic centers are shown in Figure 3.

In the D_{2h} *diamond* structures of the monoanion and trianion species, the bridging nitrogens, which define the x (horizontal) and y (vertical) axes, are the vertices of a rhombus slightly elongated along the y axis, and the pyrrole nitrogens are all equidistant from the central metal. In the case of the dianion the D_{4h} structure distorts to a D_{2h} *rectangular* structure with the thiadiazolepyrrole groups bisected by the x axis moving closer to the central metal and the perpendicular pair of thiadiazolepyrrole groups moving away, with the bridging nitrogens now forming the vertices of a square.

According to the bond parameters reported in Table 2, the $Zn-N_p$ bond slightly lengthens as the negative charge on the macrocycle increases. In the D_{2h} *rectangular* structure of the dianion, the $Zn-N_p$ bond shortens along the x axis and elongates along the perpendicular axis (see Table 2). The changes of the other bond parameters along the series can be rationalized in terms of the nodal pattern of the occupied components of the e_g* MOs. Considering first the monoanion, the changes of the bond parameters are consistent with the topology of the yz component of the e_g*, the singly occupied $8b_{3g}$ MO (SOMO, singly occupied molecular orbital) in the distorted D_{2h} diamond structure

(27) Clack, D. W.; Yandle, J. R. *Inorg. Chem.* **1972**, *11*, 1738.
(28) Englman, R. *The Jahn−Teller Effect in Molecules and Crystals*; Wiley: London, 1972.
(29) Bersuker, I. B. *Chem. Rev.* **2001**, *101*, 1067.
(30) Cory, M. G.; Hirose, H.; Zerner, M. C. *Inorg. Chem.* **1995**, *34*, 2969.
(31) Nguyen, K. A.; Pachter, R. *J. Chem. Phys.* **2003**, *118*, 5802.
(32) (a) Clack, D. W.; Hush, N. S.; Yandle, J. R. *Chem. Phys. Lett.* **1967**, *1*, 157. (b) Giraudeau, A.; Louati, A.; Gross, M.; André, J. J.; Simon, J.; Su, C. H.; Kadish, K. M. *J. Am. Chem. Soc.* **1983**, *105*, 2917. (c) Louati, A.; El Meray, M.; André, J. J.; Simon, J.; Kadish, K. M.; Gross, M.; Giraudeau, A. *Inorg. Chem.* **1985**, *24*, 1175.
(33) Dreuw, A.; Weisman, J. L.; Head-Gordon, M. *J. Chem. Phys.* **2003**, *119*, 2943.

Table 2. Symmetry Unique Bond Lengths (Å) and Angles (deg) Calculated for $[TTDPzZn]^n$ (n = 0, 1−, 2−, 3−, 4−) in the Gas-Phase[a,b]

	$[TTDPzZn]$[c] D_{4h}	$[TTDPzZn]^{\bullet 1-}$[d] D_{2h} (D)	$[TTDPzZn]^{2-}$[e] D_{2h} (R)	$[TTDPzZn]^{\bullet 3-}$[d] D_{2h} (D)	$[TTDPzZn]^{4-}$ D_{4h}
$Zn-N_p$	2.022	2.026	2.056/2.007	2.032	2.033
$C_\alpha-N_p$	1.384	1.406/1.373	1.404/1.384	1.416/1.384	1.404
$C_\alpha-C_\beta$	1.459	1.461/1.448	1.465/1.434	1.455/1.439	1.447
$C_\beta-C_\beta$	1.425	1.433	1.454/1.433	1.451	1.456
$C_\alpha-N_b$	1.323	1.331/1.321	1.356/1.307	1.338/1.331	1.339
$C_\beta-N_t$	1.328	1.334/1.327	1.341/1.329	1.345/1.334	1.347
$S-N_t$	1.650	1.656/1.655	1.674/1.652	1.677/1.675	1.690
$C_\alpha-N_p-C_\alpha$	111.3	111.4	112.1/110.8	111.2	110.9
$C_\alpha-N_b-C_\alpha$	125.1	123.4/126.0[f]	124.2	123.0/125.3[f]	124.1
N_t-S-N_t	101.1	101.1	101.9/100.0	101.1	101.1

[a] The z axis is perpendicular to the molecular plane (the xy plane). The x and y axes point to the bridging nitrogens, N_b, except in the D_{2h} *rectangular* structure of the dianion where they point to the pyrrolic nitrogens, N_p. [b] The *diamond* and *rectangular* structures are labeled by the D and R letters, respectively. [c] Data from ref 5. [d] The bond lengths in the column refer to the bonds facing the x/y axes. [e] The data in the column refer to the thiadiazolepyrrole moieties bisected by the y/x axes. [f] The data are for the $C_\alpha-N_b-C_\alpha$ bond angles bisected by the x/y axes.

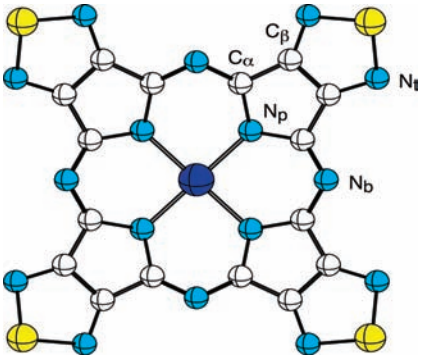

Figure 3. Atom labeling scheme for $[TTDPzZn]^n$ (n = 0, 1−, 2−, 3−, 4−).

of $[TTDPzZn]^{\bullet -}$ (see the plot of this MO in Figure 4a). For instance, the four $C_\alpha-N_p$ bonds facing the x axis elongate on account of the increased π-antibonding interaction between the C_α and N_p atoms. By contrast, the $C_\alpha-N_p$ bonds facing the y axis shorten, and that is consistent with the increased π-bonding interaction between the involved atoms. Similarly, the bonds between the C_α atoms and the N_b atoms lying on the y axis elongate significantly on account of the increased π-antibonding interaction between these atoms, while the $C_\alpha-N_b$ bonds involving the bridging nitrogens on the x axis remain unperturbed because the $8b_{3g}$ SOMO has no amplitude on the N_b atoms lying on this axis.

In turn, the geometrical changes observed for the dianion are in line with the nodal pattern of the now doubly occupied yz component of the e_g*, the $8b_{3g}$ in the distorted D_{2h} rectangular structure of this species (see the plot of this orbital Figure 4b). As an example, the $C_\alpha-N_p$ bond of the pyrroles bisected by the y axis elongates significantly, on account of the increased π-antibonding interaction between the C_α and N_p atoms. Consistent with the $8b_{3g}$ having no amplitude on the N_p atoms lying on the x axis the $C_\alpha-N_p$ bond of the pyrroles bisected by the x axis remains unperturbed. Similarly, the $S-N_t$ bond of the thiadiazole groups bisected by the y axis is significantly longer than in the neutral species (1.674 vs 1.650 Å), while the $S-N_t$ bond of the thiadiazole groups bisected by the x axis remains unchanged. Yet, this fits in with the $8b_{3g}$-HOMO being π-antibonding between the sulfur and nitrogen atoms of the thiadiazole groups bisected by the y axis and having no amplitude on the sulfur atoms on the x axis.

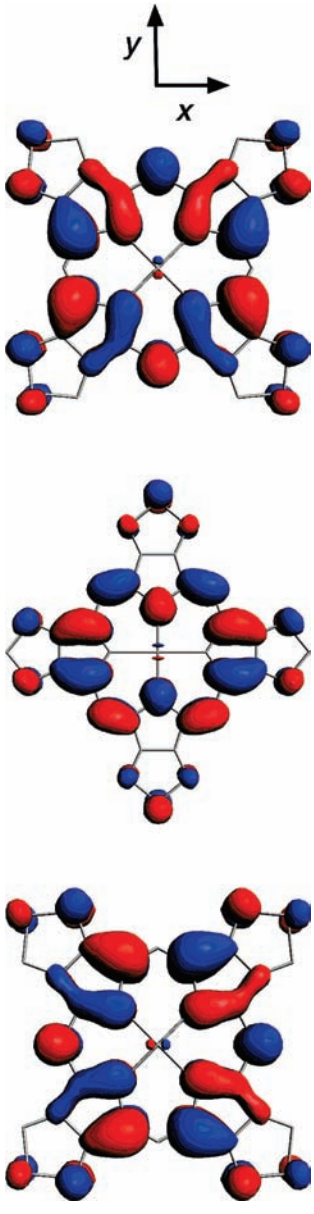

Figure 4. Plots of the (a) SOMO ($8b_{3g}\uparrow$) of $[TTDPzZn]^{\bullet -}$, (b) HOMO ($8b_{3g}$) of $[TTDPzZn]^{2-}$, and (c) SOMO ($8b_{2g}\uparrow$) of $[TTDPzZn]^{\bullet 3-}$ as obtained by DFT/B3LYP calculations in pyridine solution.

The geometrical changes observed in the trianionic and tetraanionic species can be rationalized by similar arguments by taking into account that in the former the $8b_{3g}$ (Figure 4a) is fully occupied and the $8b_{2g}$ (Figure 4c) is singly occupied, in the latter both the *yz* and *xz* components of the e_g* are fully occupied. Looking for instance at the S−N_t bond in the trianion we may observe that the four S−N_t bonds facing the *x* axis are much longer than in the monoanion (1.674 vs 1.656 Å), on account of the double occupancy of the $8b_{3g}$. The four S−N_t bonds facing the *y* axis are also longer than in the monoanion (1.675 vs 1.655 Å), which is consistent with singly occupancy of the $8b_{2g}$ increasing the π-antibonding interaction between the involved S and N_t atoms.

Excited States and Optical Spectra. To provide an interpetation of the optical spectra of $[TTDPzZn]^{n-}$ (n = 1−4) anionic complexes, we have calculated the lowest allowed excited states using TDDFT methods in conjunction with both pure, asymptotically correct (SAOP) and hybrid (B3LYP) exchange-correlation functionals. The joint use of these functionals is essential to attain a correct assignment of the key features of the spectra. We anticipate that the theoretical description of the optical spectra of these species is complicated by the presence of excitations involving MOs largely localized on the thiadiazole rings. Since these transitions create intramolecular inter-ring charge transfer processes, they are intrinsically of charge transfer (CT) nature and, in view of the well-known tendency of TDDFT methods to underestimate the energy of charge transfer (CT) transitions,[33−35] are likely to be calculated at somewhat too low an energy.[36] As a matter of fact, they either appear as "ghost states" or undergo configuration mixing with non CT transitions. The extent to which this mixing occurs depends on the energy of the involved MOs and hence varies on changing the exchange-correlation functional. In the present case the CT failure of TDDFT prevents the correct assignment of some spectral features when using the pure SAOP functional. The use of hybrid functionals with even a small fraction of Hartree−Fock (HF) exchange such as B3LYP is sufficient to remedy the CT problem of TDDFT in most of the cases here encountered. However, for excitations that are correctly given by TDDFT, the inclusion of a fraction of exact exchange deteriorates the results, as is by now well established.[37,38] In these cases SAOP provides more accurate excitation energies than B3LYP. Therefore, both the B3LYP and SAOP results will be used to interpret the optical spectra of the investigated anionic species.

$[TTDPzZn]^{\bullet-}$. As mentioned in the previous section, this species has a $^2B_{3g}$ electronic ground state in the equilibrium JT distorted D_{2h} *diamond* structure. The ground state spin density distribution in $[TTDPzZn]^{\bullet-}$ shown in Figure 5a largely reflects the atomic orbital composition of the SOMO, the $8b_{3g}^{\uparrow}$, (see Figure 4a). An appreciable (−0.030) negative spin density also resides on the p_z orbitals of the N_b atoms lying on the *x* axis and of the C_α and N_t atoms facing the *y* axis. An energy level scheme showing the highest-occupied and lowest-unoccupied Kohn-Sham (KS) spin orbitals of $[TTDPzZn]^{\bullet-}$ obtained from DFT/B3LYP/TZ2P calculations in pyridine is displayed in Figure 6. Apart from the generalized destabilization of the levels induced by the negative charge, the key features of the ground-state electronic structure of the monoanion do not differ significantly from those of the neutral species discussed in the previous paper of this series.[5] Worth mentioning in this context is the presence in the virtual spectrum, immediately above the LUMO, of a set of low-lying π* MOs largely localized on the thiadiazole moieties (see plots in Figure 7), hereafter denoted as π^*_{TD}.

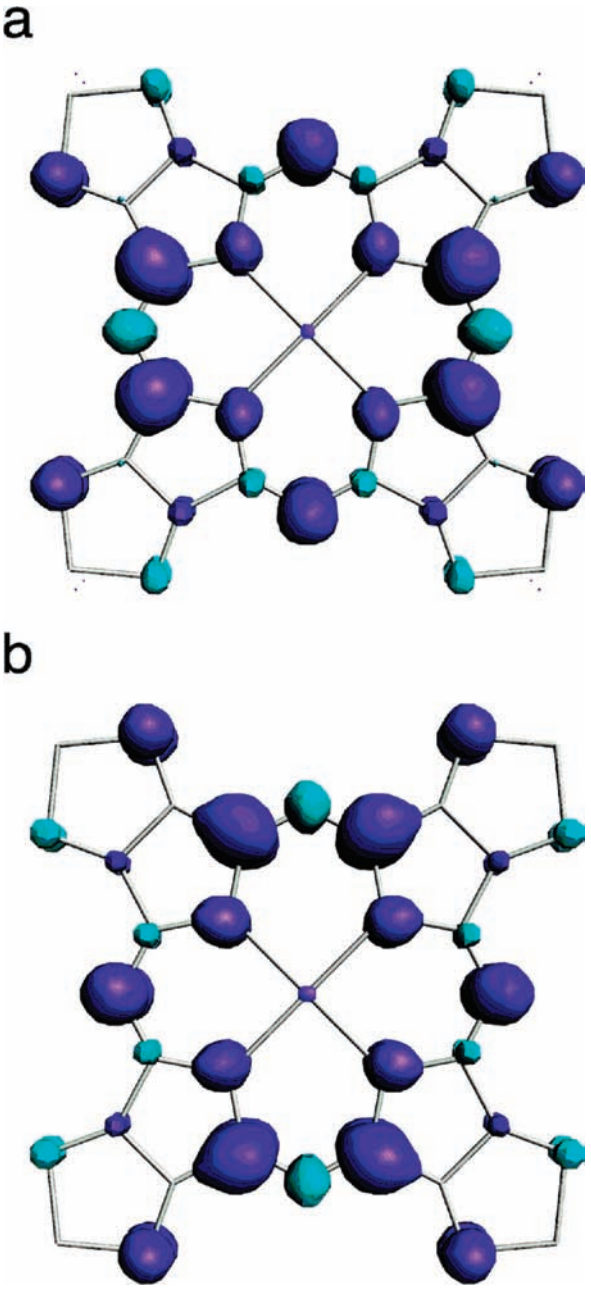

Figure 5. Spin density distribution in (a) $[TTDPzZn]^{\bullet-}$ and (b) $[TTDPzZn]^{\bullet 3-}$ as obtained from DFT/B3LYP calculations in pyridine solution. Majority and minority spin densities are shown in blue and sea-green, respectively.

(34) Dreuw, A.; Head-Gordon, M. *J. Am. Chem. Soc.* **2004**, *126*, 4007.
(35) Dreuw, A.; Head-Gordon, M. *Chem. Rev.* **2005**, *105*, 4009.
(36) Cai, Z.-L.; Crossley, M. J.; Reimers, J. R.; Kobayashi, R.; Amos, R. D. *J. Phys. Chem. B* **2006**, *110*, 15624.
(37) Magyar, R. J.; Tretiak, S. *J. Chem. Theory Comput.* **2007**, *3*, 976.
(38) Goerigk, L.; Grimme, S. *J. Phys. Chem. A* **2009**, *113*, 767.

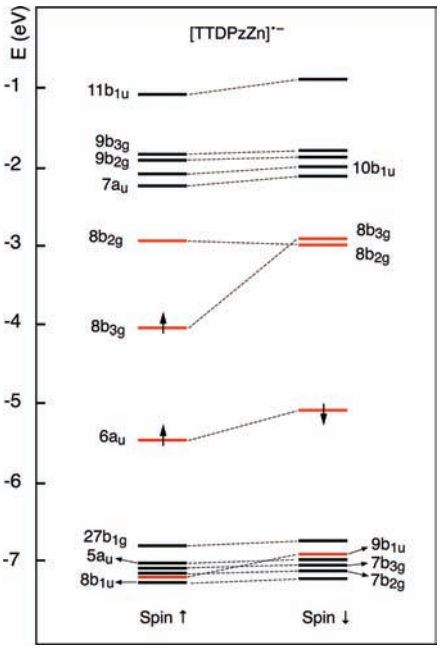

Figure 6. Energy level scheme for $[TTDPzZn]^{\bullet-}$ as obtained from spin-unrestricted DFT/B3LYP calculations in pyridine solution. The Gouterman MOs, the $9b_{1u}$, $6a_u$, $8b_{3g}$, and $8b_{2g}$, are indicated with red lines.

These low-lying π^* MOs play an important role in the absorption spectra of all anionic species here investigated. As inferred from the orbital diagram of Figure 6, the JT splitting of the e_g^* is quite small. The spin down components of the resulting $8b_{3g}$ and $8b_{2g}$ MOs are indeed nearly degenerate, the splitting of the spin up components being merely related to occupation of the $8b_{3g}$.

The absorption spectra of the electrochemically generated anionic species of the zinc complex, $[TTDPzZn]^{n-}$ ($n = 1-3$) and of the tetraanions $[TTDPzH_2]^{4-}$ and $[TTDPzCu]^{4-}$ in pyridine are illustrated in Figure 8.

The absorption spectrum of $[TTDPzZn]^{\bullet-}$ shares common features with that of the phthalocyanine analogue, namely, the presence of three prominent clusters of bands in the near-IR, visible, and near-UV regions.[28,8] The energy and intensity of the bands constituting these clusters vary significantly, however, going from the phthalocyanine to the thiadiazolporphyrazine macrocyclic complex. In particular, the near-IR and near-UV clusters are blue and red-shifted, respectively, and the *two* intense and sharp absorptions at 570 and 635 nm are replaced by an intense and sharp absorption at 554 nm and a much weaker and broadband near 670 nm. To provide an assignment of the main spectral features of $[TTDPzZn]^{\bullet-}$ we have computed the excitation energies and oscillator strengths of the dipole and spin allowed ^2A_u, $^2B_{1u}$, and $^2B_{3u}$ excited states of the complex in pyridine solution. With our choice of coordinates these states are *y*, *x*, and *z* allowed, respectively. The B3LYP and SAOP results are reported in Tables 3 and 4, respectively. The excited states having B_{3u} symmetry are not listed in the tables since they have oscillator strengths smaller than 0.001 and are therefore not relevant for the interpretation of the main spectral features. In Figure 9 the computed (TDDFT/B3LYP) and experimental absorption spectra of $[TTDPzZn]^{\bullet-}$ in pyridine are compared. The TDDFT calculations locate three excited

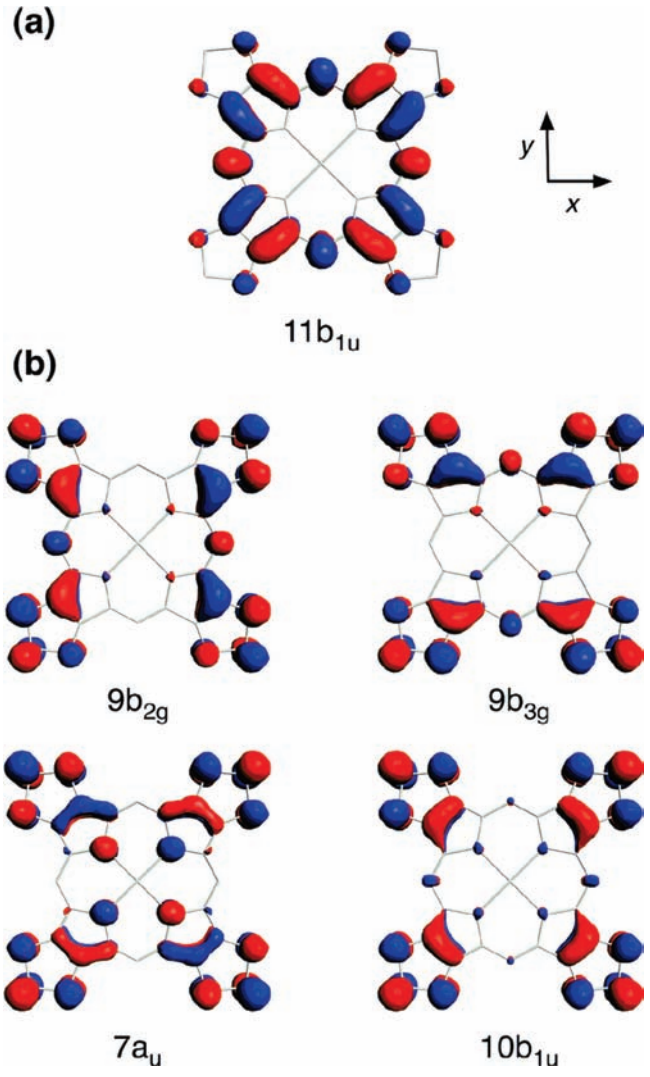

Figure 7. Plots of the (a) $11b_{1u}$ and (b) π^*_{TD} MOs of $[TTDPzZn]^{\bullet-}$ as obtained from DFT/B3LYP calculations in pyridine solution. Only the spin-up components are shown.

states in the near-IR region, one of which, the 1^2B_{1u} at B3LYP level, the 2^2B_{1u} at SAOP level, is a pure $6a_u \rightarrow 8b_{2g}$ $\pi \rightarrow \pi^*$ state. As the $6a_u \rightarrow 8b_{2g}$ transition would in the neutral species be the $2a_{1u} \rightarrow 8e_g$:*yz* that describes the *x*-polarized component of the 1^1E_u excited state accounting for the intense Q band, the $^2B_{1u}$ $\pi \rightarrow \pi$ excited state of the monoanion is denoted as Q'_x. The higher lying doublet excited state generated by the same $6a_u \rightarrow 8b_{2g}$ transition[39] is denoted as Q''_x, vide infra. The 1.36 eV (911 nm) excitation energy computed at SAOP level for the Q'_x state strongly suggests assignment of this state to the near-IR band at 895 nm. TDDFT/B3LYP calculations locate the Q'_x state ~150 nm to the red of the 895 nm band, which is consistent with the inclusion of a fraction of exact exchange providing less accurate energetics in the case of excitations that are correctly given by TDDFT because the cancellation of errors between exchange and correlation is reduced.[39]

(39) In molecular systems with a doublet ground-state one-electron transitions from fully occupied orbitals to virtual orbitals result in one set of quartet excited states and two sets of doublet excited states, whereas one-electron transitions from or into the singly occupied orbital result in doublet states.

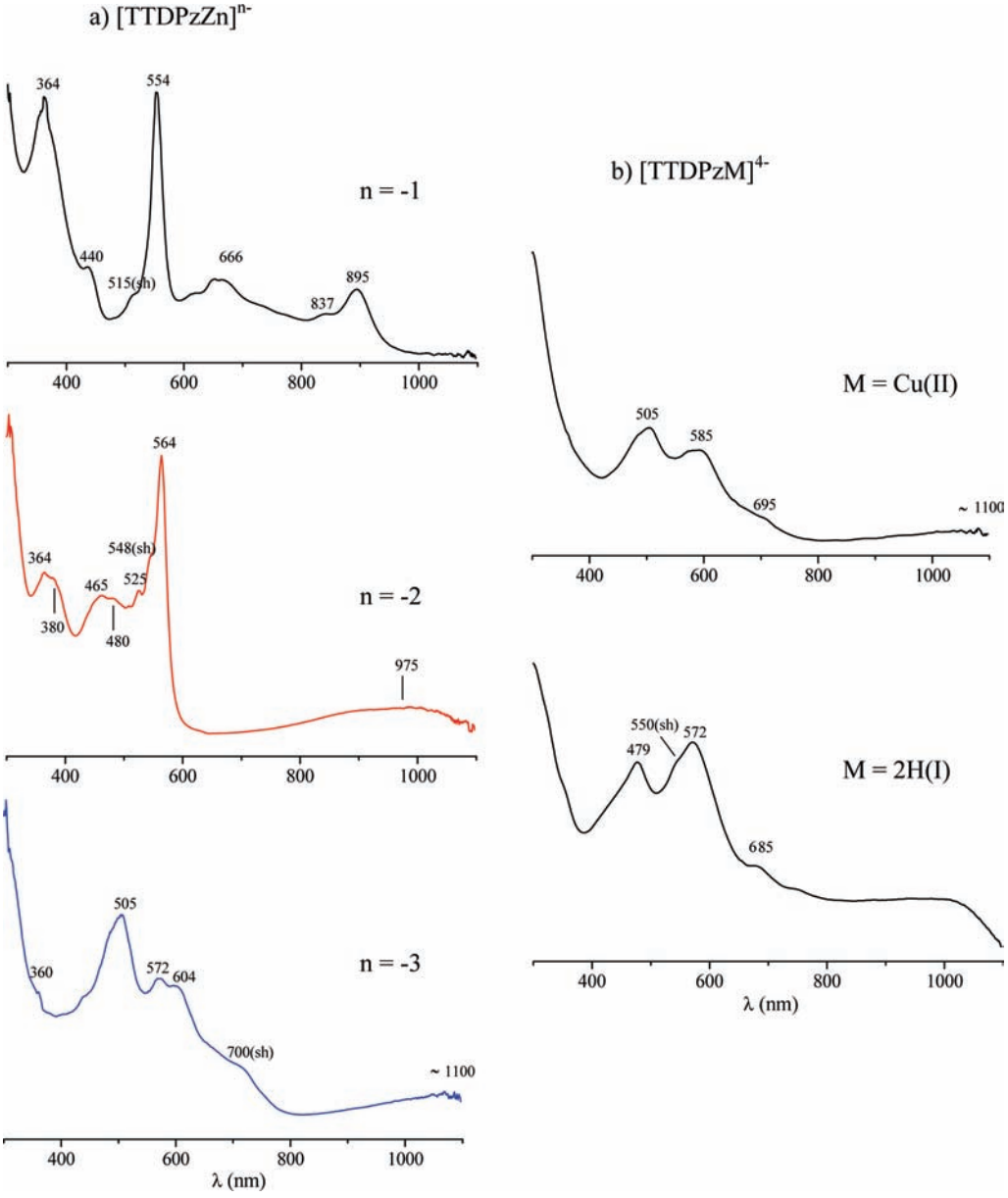

Figure 8. UV−visible spectra in pyridine of (a) $[TTDPzZn]^n$ ($n = -1, -2$, and -3) and (b) $[TTDPzM]^{4-}$ ($M = Cu^{II}$ and $= 2H^{I}$).

Two arguments lend support to the assignment of the Q'_x state to the 895 nm band: (i) this band is present only in the spectrum of the monoanion, as it should be. Indeed the $\pi \rightarrow \pi^*$ transition responsible for the Q'_x state of the monoanion should either be not active (trianion and tetranion) or generate a "normal" Q state (dianion). (ii) The 895 nm band shifts slightly to the red (956 nm) in the zinc phthalocyanine π-anion radical,[8] which is consistent with the diminished HOMO−LUMO gap going from [TTDPzZn] to [PcZn].[5]

As for the remaining excited states computed in the near-IR region, the 1^2A_u and the $1^2B_{1u}/2^2B_{1u}$ (SAOP/B3LYP), they both involve transitions from the SOMO into MOs of the π^*_{TD} set. In line with these states having some CT character, they are predicted at the SAOP level at much lower energy than at the B3LYP level. TDDFT/B3LYP calculations, which are certainly less affected by the CT problem, locate the 1^2A_u ~50 nm to the red and the 2^2B_{1u} ~100 nm to the blue of the Q'_x band, suggesting assignment of the latter to the broad feature appearing to the blue of the 895 nm band. According to the TDDFT results, the broad absorption in the visible region originates from the 2^2A_u state that is largely composed by the $6a_u\downarrow \rightarrow 8b_{3g}\downarrow$, HOMO→SOMO transition. As this transition would in the neutral species be the $2a_{1u} \rightarrow 8e_g$:*xz* that describes the *y*-polarized component of the 1^1E_u excited state accounting for the Q band, the feature appearing in the absorption spectrum of the π-anion radical at ~666 nm is denoted as Q_y. In the visible region, to the blue of the Q_y band, two excited states are theoretically predicted, the weak 3^2B_{1u} and the quite intense 4^2B_{1u}. These states arise from the mixing of the Gouterman $6a_u \rightarrow 8b_{2g}$ transition responsible for the Q'_x state with the non Gouterman $6a_u\downarrow \rightarrow 9b_{2g}\downarrow$ and $8b_{3g}\uparrow \rightarrow 11b_{1u}\uparrow$ transitions. On the basis of the calculated excitation energies and oscillator strengths, the assignment of the intense, sharp feature at 554 nm to the 4^2B_{1u} excited state is straightforward. Owing to the participation of the Gouterman $6a_u$

Table 3. TDDFT/B3LYP Vertical Excitation Energies, E (eV/nm), Computed for the Optically Allowed $^2B_{1u}$ and ^2A_u Excited States of $[TTDPzZn]^{\bullet-}$ in Pyridine[a,b,c]

state	composition (%)	E	expt[d]	state	composition (%)	E	expt[d]
1^2A_u	$8b_{3g}\uparrow\rightarrow 7a_u\uparrow$ (86) $6a_u\downarrow\rightarrow 8b_{3g}\downarrow$ (13)	1.14/1091 (0.016)		5^2B_{1u}	$6a_u\downarrow\rightarrow 9b_{2g}\downarrow$ (43) $6a_u\uparrow\rightarrow 9b_{2g}\uparrow$ (20) $8b_{3g}\uparrow\rightarrow 11b_{1u}\uparrow$ (17)	2.69/460 (0.102)	2.82/440
1^2B_{1u}	$6a_u\downarrow\rightarrow 8b_{2g}\downarrow$ (70) $6a_u\uparrow\rightarrow 8b_{2g}\uparrow$ (20)	1.19/1041 (0.001)	1.39/895 Q'_x	7^2B_{1u}	$6a_u\uparrow\rightarrow 9b_{2g}\uparrow$ (61) $6a_u\downarrow\rightarrow 9b_{2g}\downarrow$ (17)	3.02/411 (0.050)	
2^2B_{1u}	$8b_{3g}\uparrow\rightarrow 10b_{1u}\uparrow$ (91)	1.32/937 (0.025)		6^2A_u	$9b_{1u}\downarrow\rightarrow 8b_{2g}\downarrow$ (15) $9b_{1u}\uparrow\rightarrow 8b_{2g}\uparrow$ (15) $6a_u\uparrow\rightarrow 9b_{3g}\uparrow$ (11)	3.12/397 (0.050)	
2^2A_u	$6a_u\downarrow\rightarrow 8b_{3g}\downarrow$ (82) $8b_{3g}\uparrow\rightarrow 7a_u\uparrow$ (12)	1.75/710 (0.222)	~1.86/666 Q_y	9^2B_{1u}	$5a_u\uparrow\rightarrow 8b_{2g}\uparrow$ (41) $9b_{1u}\downarrow\rightarrow 8b_{3g}\downarrow$ (21)	3.54/350 (0.496)	3.41/364
3^2B_{1u}	$6a_u\uparrow\rightarrow 8b_{2g}\uparrow$ (56) $8b_{3g}\uparrow\rightarrow 11b_{1u}\uparrow$ (32)	2.15/576 (0.045)		10^2B_{1u}	$9b_{1u}\downarrow\rightarrow 8b_{3g}\downarrow$ (40) $5a_u\uparrow\rightarrow 8b_{2g}\uparrow$ (32)	3.56/348 (0.226)	B_x
4^2B_{1u}	$8b_{3g}\uparrow\rightarrow 11b_{1u}\uparrow$ (35) $6a_u\downarrow\rightarrow 9b_{2g}\downarrow$ (30) $6a_u\downarrow\rightarrow 8b_{2g}\downarrow$ (12) $6a_u\uparrow\rightarrow 8b_{2g}\uparrow$ (11)	2.40/517 (0.214)	2.24/554 Q''_x	10^2A_u	$9b_{1u}\uparrow\rightarrow 8b_{2g}\uparrow$ (34) $9b_{1u}\downarrow\rightarrow 8b_{2g}\downarrow$ (11) $8b_{1u}\uparrow\rightarrow 8b_{2g}\uparrow$ (24) $8b_{1u}\downarrow\rightarrow 8b_{2g}\downarrow$ (13)	3.83/324 (0.378)	3.41/364 B_y

[a] The major one-electron transitions contributing to the solution vectors are also given. [b] Oscillator strengths (f) in parentheses. [c] Of the excited states with vertical excitation energy larger than 2.50 eV (496 nm) only those with $f \geq 0.05$ are reported. [d] In pyridine solution, this work; absorption maxima in eV/nm.

Table 4. TDDFT/SAOP Vertical Excitation Energies, E (eV/nm), Computed for the Optically Allowed $^2B_{1u}$ and ^2A_u Excited States of $[TTDPzZn]^{\bullet-}$ in Pyridine[a,b,c]

state	composition (%)	E	expt[d]	state	composition (%)	E	expt[d]
1^2A_u	$8b_{3g}\uparrow\rightarrow 7a_u\uparrow$ (94)	0.90/1378 (0.027)		4^2B_{1u}	$6a_u\downarrow\rightarrow 9b_{2g}\downarrow$ (35) $8b_{3g}\uparrow\rightarrow 11b_{1u}\uparrow$ (30) $6a_u\uparrow\rightarrow 8b_{2g}\uparrow$ (13) $6a_u\downarrow\rightarrow 8b_{2g}\downarrow$ (12)	2.20/563 (0.124)	2.24/554 Q''_x
1^2B_{1u}	$8b_{3g}\uparrow\rightarrow 10b_{1u}\uparrow$ (99)	0.98/1261 (0.017)		6^2B_{1u}	$6a_u\uparrow\rightarrow 9b_{2g}\uparrow$ (29) $6a_u\downarrow\rightarrow 9b_{2g}\downarrow$ (21) $9b_{1u}\downarrow\rightarrow 8b_{3g}\downarrow$ (14)	2.65/467 (0.137)	2.82/440
2^2B_{1u}	$6a_u\downarrow\rightarrow 8b_{2g}\downarrow$ (63) $6a_u\uparrow\rightarrow 8b_{2g}\uparrow$ (36)	1.36/911 (0.001)	1.39/895 Q'_x	8^2B_{1u}	$a_u\uparrow\rightarrow 8b_{2g}\uparrow$ (50) $5a_u\downarrow\rightarrow 8b_{2g}\downarrow$ (31)	2.85/435 (0.059)	
2^2A_u	$6a_u\downarrow\rightarrow 8b_{3g}\downarrow$ (89)	1.72/723 (0.152)	~1.86/666 Q_y	11^2B_{1u}	$8b_{1u}\downarrow\rightarrow 8b_{3g}\downarrow$ (39) $9b_{1u}\downarrow\rightarrow 8b_{3g}\downarrow$ (20)	3.33/372 (0.675)	3.41/364 B_x
3^2B_{1u}	$8b_{3g}\uparrow\rightarrow 11b_{1u}\uparrow$ (47) $6a_u\uparrow\rightarrow 8b_{2g}\uparrow$ (38) $6a_u\downarrow\rightarrow 8b_{2g}\downarrow$ (14)	1.78/696 (0.014)		10^2A_u	$8b_{1u}\uparrow\rightarrow 8b_{2g}\uparrow$ (36) $8b_{1u}\downarrow\rightarrow 8b_{2g}\downarrow$ (15) $8b_{3g}\uparrow\rightarrow 8a_u\uparrow$ (18)	3.38/367 (0.232)	3.41/364 B_y

[a] The major one-electron transitions contributing to the solution vectors are also given. [b] Oscillator strengths (f) in parentheses. [c] Of the excited states with vertical excitation energy larger than 2.50 eV (496 nm) only those with $f \geq 0.05$ are reported. [d] In pyridine solution, this work; absorption maxima in eV/nm.

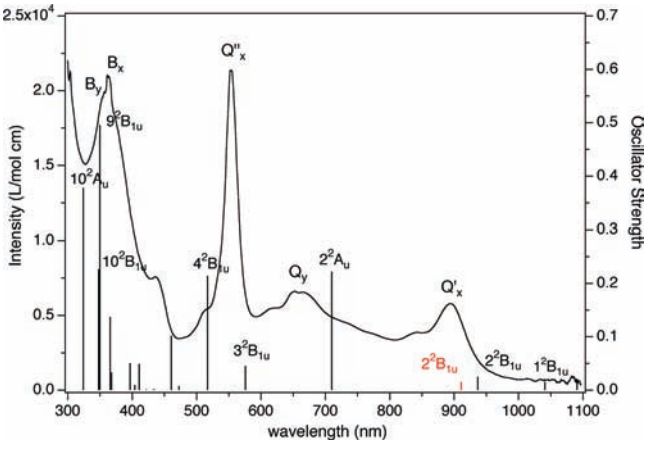

Figure 9. Computed (TDDFT/B3LYP) and experimental (this work) absorption spectra of $[TTDPzZn]^{\bullet-}$ in pyridine. The 2^2B_{1u} excited state (TDDFT/SAOP) that accounts for the Q'_x band is also reported (red stick) in the figure (see text for a discussion on the assignment of this band).

$\rightarrow 8b_{2g}$ transition to the composition of 4^2B_{1u}, this state is denoted as Q''_x. Coming now to the near-UV cluster, the quite intense feature at 440 nm, appearing as a distinct shoulder of the very intense 364 nm band, is assigned to the $6^2B_{1u}/5^2B_{1u}$ (SAOP/B3LYP) excited state generated by a transition from the HOMO into an MO of the π^*_{TD} set. In the B band region TDDFT/SAOP results locate two intense, close lying excited states, the 11^2B_{1u} and 10^2A_u, at 372 and 367 nm, respectively, in nice agreement with the experiment. These states are the x and y components of the E_u state accounting for the B band in the neutral complex and are therefore denoted as B_x and B_y. As can be inferred from their composition, these excited states arise from transitions out of the a_{2u}-derived Gouterman MO, the $8b_{1u}$ according to DFT/SAOP results, the $9b_{1u}$ according to DFT/B3LYP results, into the SOMO (11^2B_{1u}) and LUMO (10^2A_u). TDDFT/B3LYP calculations provide substantially the same description of the B band, save for the splitting of the B_x component into two states, the 9^2B_{1u} and 10^2B_{1u}, due to the mixing of the $9b_{1u}\downarrow\rightarrow 8b_{3g}\downarrow$ and $5a_u\downarrow\rightarrow 8b_{2g}\downarrow$ transitions.

$[TTDPzZn]^{2-}$. The absorption spectrum of the dianionic species shows (see Figure 8) a very broad, weak absorption in the near-IR region (800−1100 nm), an intense band in the visible region centered at 564 nm followed by a cluster of bands, and a prominent absorption in the

Table 5. TDDFT/B3LYP Vertical Excitation Energies, E (eV/nm), Computed for the Optically Allowed $^1B_{2u}$ and $^1B_{3u}$ Excited States of $[TTDPzZn]^{2-}$ in Pyridine[a,b]

state	composition (%)	*E*	expt[c]	state	composition[a] (%)	*E*	expt[c]
1^1B_{2u}	$8b_{3g} \rightarrow 12b_{1u}$ (62) $8b_{3g} \rightarrow 13b_{1u}$ (34)	1.21/1023 (0.068)	~1.27/975	2^1B_{3u}	$4a_u \rightarrow 9b_{3g}$ (57) $8b_{3g} \rightarrow 5a_u$ (32)	2.88/431 (0.263)	2.68/462
2^1B_{2u}	$8b_{3g} \rightarrow 13b_{1u}$ (65) $8b_{3g} \rightarrow 12b_{1u}$ (32)	1.28/969 (0.051)		4^1B_{2u}	$4a_u \rightarrow 9b_{2g}$ (91)	3.18/390 (0.370)	3.26/380
3^1B_{2u}	$4a_u \rightarrow 8b_{2g}$ (88)	2.34/529 (0.383)	2.20/564 *Q*	3^1B_{3u}	$11b_{1u} \rightarrow 8b_{2g}$ (54) $10b_{1u} \rightarrow 8b_{2g}$ (28)	3.73/333 (0.450)	3.41/364 *B*
1^1B_{3u}	$8b_{3g} \rightarrow 5a_u$ (59) $4a_u \rightarrow 9b_{3g}$ (39)	2.64/470 0.094)	2.58/480				

[a] The major one-electron transitions contributing to the solution vectors are also given. [b] Oscillator strengths in parentheses. [c] In pyridine solution, this work; absorption maxima in eV/nm.

Table 6. TDDFT/SAOP Vertical Excitation Energies (eV/nm) Computed for the Optically Allowed $^1B_{2u}$ and $^1B_{3u}$ Excited States of $[TTDPzZn]^{2-}$ in Pyridine[a,b,c]

state	composition (%)	*E*	expt[d]	state	composition[a] (%)	*E*	expt[d]
1^1B_{2u}	$8b_{3g} \rightarrow 13b_{1u}$ (79) $8b_{3g} \rightarrow 12b_{1u}$ (18)	0.89/1393 (0.006)	~1.27/975	2^1B_{3u}	$4a_u \rightarrow 9b_{3g}$ (53) $8b_{3g} \rightarrow 5a_u$ (29)	2.51/494 (0.167)	2.68/462
2^1B_{2u}	$8b_{3g} \rightarrow 12b_{1u}$ (74) $8b_{3g} \rightarrow 13b_{1u}$ (20)	0.97/1273 (0.073)		4^1B_{2u}	$4a_u \rightarrow 9b_{2g}$ (78) $4a_u \rightarrow 8b_{2g}$ (13)	2.66/466 (0.359)	3.26/380
3^1B_{2u}	$4a_u \rightarrow 8b_{2g}$ (74) $4a_u \rightarrow 9b_{2g}$ (18)	2.05/604 (0.240)	2.20/564 *Q*	3^1B_{3u}	$11b_{1u} \rightarrow 8b_{2g}$ (86)	2.92/425 (0.076)	
1^1B_{3u}	$8b_{3g} \rightarrow 5a_u$ (56) $4a_u \rightarrow 9b_{3g}$ (41)	2.09/593 (0.050)	2.58/480	6^1B_{3u}	$10b_{1u} \rightarrow 8b_{2g}$ (39) $9b_{1u} \rightarrow 8b_{2g}$ (25) $10b_{1u} \rightarrow 9b_{2g}$ (14)	3.51/353 (0.523)	3.41/364 *B*

[a] The major one-electron transitions contributing to the solution vectors are also given. [b] Oscillator strengths (*f*) in parentheses. [c] Of the excited states with vertical excitation energy larger than 2.75 eV (450 nm) only those with $f \geq 0.05$ are reported. [d] In pyridine solution, this work; absorption maxima in eV/nm.

B band region. The excitation energies and oscillator strengths computed for the dipole and spin allowed $^1B_{2u}$ and $^1B_{3u}$ excited states of the dianionic species are gathered in Tables 5 and 6. The excited states of B_{1u} symmetry are not listed in the Tables since they have oscillator strengths smaller than 0.001 and are therefore not relevant for the interpretation of the main spectral features. An energy level scheme showing the highest occupied and lowest unoccupied KS orbitals obtained from DFT/B3LYP/TZ2P calculations in pyridine is displayed in Figure 10.

In the near−IR region TDDFT calculations locate only two optically allowed excited states of moderate intensity, the 1^1B_{2u} and 2^1B_{2u}. According to their composition, these states result from the mixing of two $\pi^* \rightarrow \pi^*$ transitions, the $8b_{3g} \rightarrow 12b_{1u}$ and $8b_{3g} \rightarrow 13b_{1u}$. The 1^1B_{2u} and 2^1B_{2u} excited states, which are computed at B3LYP level at 1023 and 969 nm, respectively, are responsible for the broad near, IR absorption with maximum at ~975 nm (see Figure 11). TDDFT/SAOP calculations significantly underestimate the excitation energy of these excited states, which is consistent with their partial CT character, they involve transitions out of the $8b_{3g}$−HOMO into MOs of the π^*_{TD} set (see level scheme of Figure 10). In agreement with the experiment, no excited states are predicted up to ~600 nm, the next excited state, the intense 3^1B_{2u}, being computed at 604 nm at the SAOP level and at 529 nm at the B3LYP level. The excitation energy and oscillator strength of the 3^1B_{2u} leave no doubt on the assignment of this state to the intense spectral

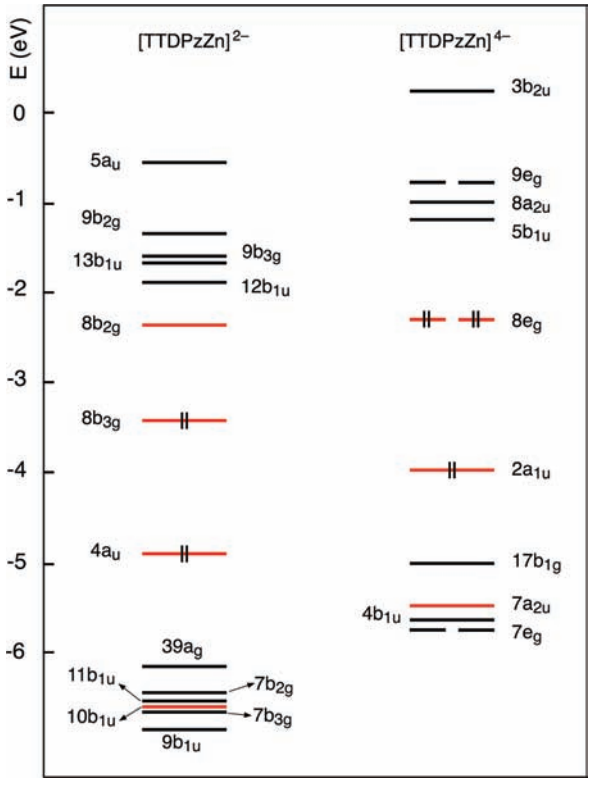

Figure 10. Energy level scheme for $[TTDPzZn]^{2-}$ and $[TTDPzZn]^{4-}$ as obtained from DFT/B3LYP calculations in pyridine solution. The Gouterman MOs, the $10b_{1u}$, $4a_u$, $8b_{3g}$, and $8b_{2g}$ for the dianion, the $7a_{2u}$, $2a_{1u}$, and $8e_g$ for the tetraanion, are indicated with red lines.

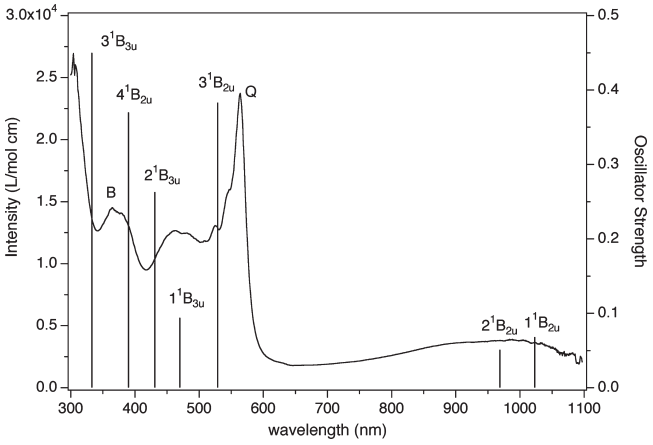

Figure 11. Computed (TDDFT/B3LYP) and experimental (this work) absorption spectra of $[TTDPzZn]^{2-}$ in pyridine.

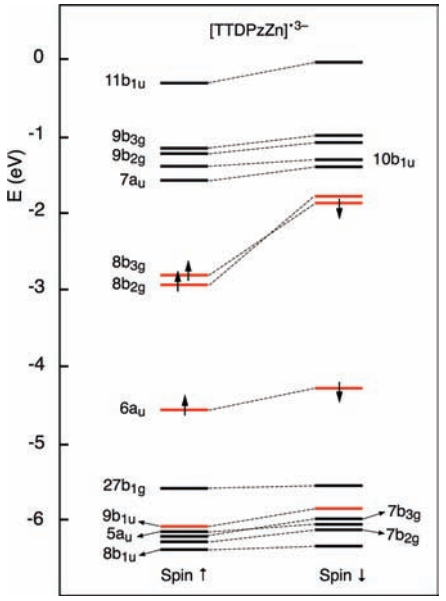

Figure 12. Energy level scheme for $[TTDPzZn]^{\bullet 3-}$ as obtained from spin-unrestricted DFT/B3LYP calculations in pyridine solution. The Gouterman MOs, the $9b_{1u}$, $6a_u$, $8b_{3g}$, and $8b_{2g}$, are indicated with red lines.

feature peaking at 564 nm. As the 3^1B_{2u} is a nearly pure $4a_u \rightarrow 8b_{2g}$ $\pi \rightarrow \pi^*$ excited state, the 564 nm band can be identified as the Q band of the dianion.

In the energy regime of the cluster of bands to blue of the Q band TDDFT/B3LYP calculations locate only two excited states, the 1^1B_{3u} and 2^1B_{3u}.

On the basis of the calculated excitation energy and oscillator strength, these states are plausible candidates for assignment to the spectral features at 480 and 462 nm. As inferred from their composition, these states arise from the mixing of the $4a_u \rightarrow 9b_{3g}$ $\pi \rightarrow \pi^*$ and $8b_{3g} \rightarrow 5a_u$ $\pi^* \rightarrow \pi^*$ transitions. Because of their partial CT character, the $4a_u \rightarrow 9b_{3g}$ transition is from a delocalized MO, the Gouterman $4a_u$, into localized MO of the π^*_{TD} set, the $9b_{3g}$, the 1^1B_{3u} and 2^1B_{3u} are calculated at a much lower energy at SAOP level. The theoretical results suggest that the shoulders of the Q band at 548 and 525 nm have a vibrational origin.

Both B3LYP and SAOP results identify the 364 nm peak as the B band. The excited state responsible for this band, the $3^1B_{3u}/6^1B_{3u}$ (B3LYP/SAOP) is indeed largely composed by a transition out of the a_{2u}-derived MO into the $8b_{2g}$-LUMO. According to B3LYP results, the intense feature immediately to the red of the B band, at 380 nm, is well accounted for by the intense 4^1B_{2u} state computed at 390 nm. As can be inferred from the composition of this state, the feature at 380 nm mainly originates from a transition out of the $4a_u$ into an MO of the π^*_{TD} set, and, as expected, is not well reproduced at SAOP level.

$[TTDPzZn]^{\bullet 3-}$. The trianionic species has a $^2B_{2g}$ electronic ground state in the equilibrium JT distorted D_{2h} *diamond* structure, the unpaired electron residing on the spin up component of the $8b_{2g}$ (see energy level scheme in Figure 12).

As shown in Figure 5b, the ground state spin density distribution in the complex largely reflects the atomic orbital composition of the SOMO (see Figure 4c). A small minority spin density resides on the p_z orbitals of the N_b atoms lying on the *y* axis and of the C_α and N_t atoms facing the *x* axis.

The absorption spectrum of the trianionic species shows (Figure 8) a weak and broad absorption in the near-IR region around 1100 nm, a cluster of absorptions in the visible consisting of a rather weak and broadband extending from ~ 750 nm to ~650 nm followed by three intense absorptions at 604, 572, and 505 nm, as well as a prominent shoulder in the B band region, at 360 nm. The TDDFT/SAOP description of the absorption spectrum of the trianionic species is greatly affected by the CT problem so as to render difficult the interpretation of the spectral features. Therefore, the interpretation of the salient spectral features of $[TTDPzZn]^{\bullet 3-}$ relies only on the TDDFT/B3LYP results reported in Table 7 and compared to the experiment in Figure 13.

For sake of completeness the SAOP results are provided in the Supporting Information, Table S3. Table 7 and Supporting Information, Table S3 list the excitation energies and oscillator strengths calculated for the dipole and spin allowed ^2A_u, $^2B_{1u}$ excited states of the trianionic species. The dipole and spin allowed excited states of B_{3u} symmetry have also been calculated, but are not reported in the tables because they have oscillator strengths smaller than 0.001.

According to the TDDFT/B3LYP results the weak and broad absorption in the near-IR region, at ~1100 nm, originates from $\pi^* \rightarrow \pi^*$ transitions out of the fully occupied $8b_{3g}$ into MOs of the π^*_{TD} set, as can be inferred from the composition of the excited states accounting for this feature, the 3^2A_u and 3^2B_{1u} which are computed at 1189 and 1149 nm, respectively. Owing to their partial CT character these states are computed at the SAOP level at far too low energy (see Supporting Information, Table S3). In the energy regime of the rather weak, broad absorption extending from ~750 nm to ~650 nm only one excited state of appreciably intensity is computed, the 5^2A_u. This state is largely described by the $6a_u{\downarrow} \rightarrow 8b_{2g}{\downarrow}$ transition and hence can be identified as the Q state of the trianion. The featureless shape of the Q band of the trianion results, most likely, from convolution of the Q(0,0) band and higher

Table 7. TDDFT/B3LYP Vertical Excitation Energies (eV/nm) Computed for the Optically Allowed $^2B_{1u}$ and ^2A_u Excited States of $[TTDPzZn]^{\bullet 3-}$ in Pyridine [a,b,c]

state	composition (%)	*E*	expt[d]	state	Composition (%)	*E*	expt[d]
3^2A_u	$8b_{3g}\downarrow \rightarrow 10b_{1u}\downarrow$ (60) $8b_{3g}\uparrow \rightarrow 10b_{1u}\uparrow$ (30)	1.04/1189 (0.052)		6^2B_{1u}	$6a_u\uparrow \rightarrow 9b_{3g}\uparrow$ (54) $6a_u\downarrow \rightarrow 9b_{3g}\downarrow$ (33)	2.85/436 (0.081)	
3^2B_{1u}	$8b_{3g}\downarrow \rightarrow 7a_u\downarrow$ (55) $8b_{3g}\uparrow \rightarrow 7a_u\uparrow$ (21) $8b_{2g}\uparrow \rightarrow 10b_{1u}\uparrow$ (19)	1.08/1149 (0.126)	~1.13/1100	8^2A_u	$6a_u\uparrow \rightarrow 9b_{2g}\uparrow$ (36) $6a_u\downarrow \rightarrow 9b_{2g}\downarrow$ (19) $8b_{3g}\downarrow \rightarrow 11b_{1u}\downarrow$ (10) $8b_{3g}\uparrow \rightarrow 11b_{1u}\uparrow$ (10)	2.99/415 (0.466)	
5^2A_u	$6a_u\downarrow \rightarrow 8b_{2g}\downarrow$ (64) $8b_{3g}\downarrow \rightarrow 11b_{1u}\downarrow$ (24)	1.95/637 (0.054)	~1.77/700 *Q*	9^2A_u	$7b_{2g}\uparrow \rightarrow 7a_u\uparrow$ (14) $7b_{2g}\downarrow \rightarrow 7a_u\downarrow$ (12) $5a_u\downarrow \rightarrow 8b_{2g}\downarrow$ (13) $7b_{3g}\uparrow \rightarrow 10b_{1u}\uparrow$ (10) $6a_u\uparrow \rightarrow 9b_{2g}\uparrow$ (10)	3.06/405 (0.242)	
4^2B_{1u}	$8b_{2g}\uparrow \rightarrow 11b_{1u}\uparrow$ (82) $6a_u\downarrow \rightarrow 9b_{3g}\downarrow$ (10)	2.03/611 (0.179)	2.05/604	8^2B_{1u}	$9b_{1u}\downarrow \rightarrow 8b_{2g}\downarrow$ (65) $8b_{3g}\uparrow \rightarrow 8a_u\uparrow$ (10)	3.38/367 (0.187)	3.44/360 *B*
7^2A_u	$6a_u\uparrow \rightarrow 9b_{2g}\uparrow$ (47) $6a_u\downarrow \rightarrow 9b_{2g}\downarrow$ (10) $8b_{3g}\uparrow \rightarrow 11b_{1u}\uparrow$ (25) $8b_{3g}\downarrow \rightarrow 11b_{1u}\downarrow$ (14)	2.50/495 (0.205)	2.46/505				

[a] The major one-electron transitions contributing to the solution vectors are also given. [b] Oscillator strengths (*f*) in parentheses. [c] Only excited states with $f \geq 0.05$ are reported. [d] In pyridine solution, this work; absorption maxima in eV/nm.

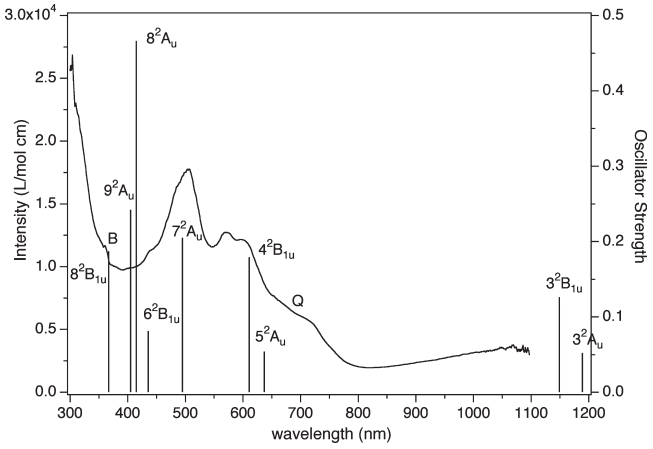

Figure 13. Computed (TDDFT/B3LYP) and experimental (this work) absorption spectra of $[TTDPzZn]^{\bullet 3-}$ in pyridine.

energy vibrational components. Notably, the Q_y band of the monoanion and the Q band of the trianion, which is also *y* polarized, share a common electronic origin. The excited states accounting for these features, the 2^2A_u in the case of the monoanion, the 5^2A_u in the case of the trianion, are both largely described by a transition out of the $6a_u$ (the HOMO of the neutral complex) into the SOMO.

In the region of the observed spectrum between 650 and 400 nm where the three intense absorptions at 604, 572, and 505 nm occur, we compute four excited states of sufficient intensity to be easily observed, the 4^2B_{1u}, 7^2A_u, 8^2A_u, and 9^2A_u. The 4^2B_{1u} and 7^2A_u can be assigned to the 604 and 572 nm features, while the 8^2A_u and 9^2A_u pair of states can be assigned to the intense and broad feature peaking at 505 nm, although the energy of the features at 572 and 505 nm is somewhat overestimated theoretically. The relative intensity pattern of the 4^2B_{1u}, 7^2A_u, 8^2A_u, and 9^2A_u excited states matches very well, however, that observed. As can be inferred from their composition in Table 7, these excited states all have a mixed $\pi \rightarrow \pi^*$ and $\pi^* \rightarrow \pi^*$ character.

TDDFT calculations unambiguously identify the prominent shoulder at 360 nm as the B band. Both the energy and intensity of the feature at 360 nm is well accounted for by the 8^2B_{1u} excited state, which is largely described by the transition out of the Gouterman $9b_{1u}$ into the SOMO.

[TTDPzZn]$^{4-}$. The absorption spectrum of $[TTDPzZn]^{4-}$ is not available because the tetraanionic species of the zinc complex could not be generated electrochemically. However, the absorption spectrum of $[TTDPzZn]^{4-}$ it not expected to differ significantly from those of the free base and copper analogues, $[TTDPzH_2]^{4-}$ and $[TTDPzCu]^{4-}$, which indeed share common features (see Figure 8). As can be inferred from the absorption spectra in Figure 8 formation of the tetraanion results in a simplification of the overall spectrum. Just as observed in the case of the phthalocyanine analogues,[28,8] going from the trianion to the tetraanion, the near-IR bands almost disappear while intense absorptions in the visible and ultraviolet region remain. As apparent from the absorption spectra of $[TTDPzH_2]^{4-}$ and $[TTDPzCu]^{4-}$ in Figure 8, the visible region is characterized by two intense absorptions whose energy and relative intensity vary with the central metal.

According to the TDDFT results gathered in Table 8, these features are accounted for by the 3^1E_u and 4^1E_u excited states computed at 543 and 435 nm at B3LYP level, at 642 and 479 nm at SAOP level. The calculated excitation energies compare well with the experimental data obtained for $[TTDPzH_2]^{4-}$ and $[TTDPzCu]^{4-}$, while the intensity pattern predicted for $[TTDPzZn]^{4-}$ matches that observed for the copper complex (see Figure 14). The 3^1E_u and 4^1E_u excited states result from the mixing of the $8e_g \rightarrow 3b_{2u}$ $\pi^* \rightarrow \pi^*$ and the $2a_{1u} \rightarrow 9e_g$ $\pi \rightarrow \pi^*_{TD}$ one-electron transitions (for the labeling of the lowest unoccupied and highest occupied MOs of $[TTDPzZn]^{4-}$ see the level scheme of Figure 10) and hence have the same electronic origin as the excited states accounting for the intense 505 and 572 nm features observed in the spectrum of the trianionic species. This explains why these features remain after the fourth reduction has occurred. In near-IR region TDDFT calculations locate two excited states,

Table 8. Vertical Excitation Energies (eV/nm) Computed for the Optically Allowed ^1E_u Excited States of $[TTDPzZn]^{4-}$ in Pyridine[a,b]

B3LYP			SAOP			
state	composition (%)	*E*	state	composition (%)	*E*	expt
1^1E_u	$8e_g \rightarrow 5b_{1u}$ (54)	0.61/2017	1^1E_u	$8e_g \rightarrow 8a_{2u}$ (61)	0.55/2254	
	$8e_g \rightarrow 8a_{2u}$ (46)	(0.007)		$8e_g \rightarrow 5b_{1u}$ (39)	(0.001)	
2^1E_u	$8e_g \rightarrow 8a_{2u}$ (52)	0.95/1311	2^1E_u	$8e_g \rightarrow 5b_{1u}$ (57)	0.88/1409	~1.13/1100[c,d]
	$8e_g \rightarrow 5b_{1u}$ (42)	(0.237)		$8e_g \rightarrow 8a_{2u}$ (36)	(0.212)	
3^1E_u	$8e_g \rightarrow 3b_{2u}$ (77)	2.28/543	3^1E_u	$8e_g \rightarrow 3b_{2u}$ (56)	1.93/642	2.17/572[c];
	$2a_{1u} \rightarrow 9e_g$ (19)	(0.451)		$2a_{1u} \rightarrow 9e_g$ (43)	(0.112)	2.12/585[d]
4^1E_u	$2a_{1u} \rightarrow 9e_g$ (78)	2.85/435	4^1E_u	$2a_{1u} \rightarrow 9e_g$ (53)	2.71/457	2.59/479[c];
	$8e_g \rightarrow 3b_{2u}$ (16)	(0.992)		$8e_g \rightarrow 3b_{2u}$ (34)	(1.043)	2.46/505[d]

[a] The major one-electron transitions contributing to the solution vectors are also given. [b] Oscillator strengths in parentheses. [c] Data for $[TTDPzH_2]^{4-}$ in pyridine solution, this work; absorption maxima in eV/nm. [d] Data for $[TTDPzCu]^{4-}$ in pyridine solution, this work; absorption maxima in eV/nm.

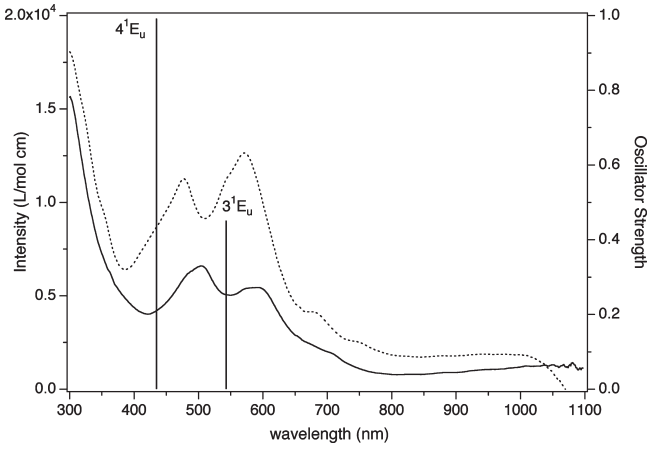

Figure 14. Comparison between the computed (TDDFT/B3LYP) absorption spectrum of $[TTDPzZn]^{4-}$ and the experimental (this work) absorption spectra of $[TTDPzCu]^{4-}$ and $[TTDPzH_2]^{4-}$ in pyridine.

the 1^1E_u and 2^1E_u, arising from the mixing of one-electron transitions out of the $8e_g$−HOMO into MOs of the π^*_{TD} set. The 2^1E_u computed at B3LYP level at 1311 nm − this state shifts to lower energy (1409 nm) at SAOP level, as expected − has appreciable intensity to be observed. According to the theoretical results, the weak feature appearing at around 700 nm in the absorption spectra of $[TTDPzH_2]^{4-}$ and $[TTDPzCu]^{4-}$ is likely to be due to trace amounts of the trianionic species as no excited states, either of E_u or of A_{2u} symmetry (the lowest $^1A_{2u}$ state is computed at 458 nm) are predicted in this spectral region.

Conclusions

UV−visible and near-IR spectra of the tetrakis(thiadiazole)porphyrazine anions $[TTDPzM]^{n-}$ ($n = 1-4$) (M = Zn^{II}, $Mg^{II}(H_2O)$, Cu^{II}, $2H^I$) were obtained by thin-layer spectroelectrochemistry in pyridine, and the ground- and excited-state properties of the electrochemically generated anionic species theoretically investigated by DFT/TDDFT methods for $[TTDPzZn]^{n-}$ ($n = 1-4$) taken as representative of the series of anionic complexes. Two exchange-correlation functionals were employed in the excited state calculations, the pure, asymptotically correct, SAOP, and the hybrid B3LYP. The use of these two functionals proved to be essential to attain a correct assignment of the key features of the spectra. In fact, the theoretical description of the optical spectra of these species is complicated by the presence of excitations involving MOs largely localized on the thiadiazole rings. Since these transitions create intramolecular inter-ring charge transfer processes, they are intrinsically of CT nature and hence are calculated at the TDDFT level at somewhat too low an energy which prevented the correct assignment of some spectral features when using the pure SAOP functional. The use of a hybrid functional with even a small fraction of Hartree−Fock (HF) exchange such as B3LYP was sufficient to remedy the CT problem of TDDFT in most of the encountered cases. On the other hand, for excitations which are correctly given by TDDFT, the inclusion of a fraction of exact exchange lowered the quality of the results. In these cases SAOP provided more accurate excitation energies than B3LYP.

Acknowledgment. Financial support by the Universities of Basilicata (Potenza) and La Sapienza (Rome), the Italian MIUR (PRIN 2007XWBRR4), and the Robert A. Welch Foundation (K.M.K, Grant E-680) is gratefully acknowledged. M.P.D. expresses her gratitude to the Dept. of Chemistry, Houston University, for kind hospitality.

Supporting Information Available: Half-wave potentials ($E_{1/2}$, V vs SCE) of the species [TTDPzM] (M = $Mg^{II}(H_2O)$, Zn^{II}, Cu^{II}, $2H^I$)[5] and phthalocyanine analogues in pyridine, DMSO, or DMF solution (0.1 M TBAP; scan rate = 100 mV/s) (Table S1), UV−visible spectral changes in pyridine for the processes $[TTDPzCu]^{2-} \rightarrow [TTDPzCu]^{1-}$ and $[TTDPzCu]^{1-} \rightarrow$ [TTDPzCu] (Figure S1), selected geometrical parameters computed for the $[TTDPzZn]^{n-}$ ($n = 1-4$) complexes in the gas-phase and in pyridine solution (Table S2). TDDFT/SAOP results for $[TTDPzZn]^{\bullet 3-}$ (Table S3). Cartesian coordinates of the gas-phase optimized structures of the $[TTDPzZn]^{n-}$ ($n = 1-4$) complexes. This material is available free of charge via the Internet at http://pubs.acs.org.